Electro-osmotic flow along superhydrophobic surfaces with embedded electrodes

Clarissa Schönecker*
Max-Planck-Institut für Polymerforschung, Mainz, Germany

Steffen Hardt
Institiute for Nano- and Microfluidics, Center of Smart Interfaces, Technische Universität Darmstadt, Germany

(Received 6 December 2013; revised manuscript received 6 March 2014; published 6 June 2014)

The effect of the secondary fluid enclosed in the indentations of a superhydrophobic surface on electro-osmotic flow is investigated. We derive analytical expressions for the net electro-osmotic flow over periodically structured surfaces, accounting for the influence of dissipation within the secondary fluid as well as for the role of charges at the fluid-fluid interfaces that are generated by auxiliary electrodes. Specifically, for a surface with rectangular grooves, the electro-osmotic flow velocity is related to the geometric parameters of the surface and the viscosity of an arbitrary secondary fluid filling the grooves. The results suggest that on specific superhydrophobic surfaces a flow enhancement by more than two orders of magnitude compared to unstructured surfaces can be expected.

DOI: 10.1103/PhysRevE.89.063005 PACS number(s): 47.55.dr, 47.65.−d, 68.08.Bc, 83.50.Lh

I. INTRODUCTION

Micro- and nanostructured surfaces in the Cassie state can exhibit an effective slippage significantly facilitating flow along the surface, an effect that especially applies to superhydrophobic surfaces. While this effect has been widely explored for shear- or pressure-driven flow (see, e.g., [1–6]), the question is to what extend this is also true for electro-osmotic flow (EOF). Previous work has addressed this question rather theoretically, modeling the fluid-fluid interfaces spanning the surface indentations by a given, yet unspecific, local slip length and local surface charge [7–9]. It has been shown that structured surfaces can only lead to a flow enhancement if the fluid-fluid interfaces carry a net charge [7,8]. However, strong doubts remain about whether it is reasonable to assume that such a net charge exists *a priori*. Within an electrolyte, any charge at an interface should attract an opposite charge forming a Debye layer. Consequently, the interface is effectively neutral over a scale of the Debye layer thickness. The electrokinetic movements of the charges at a fluid-fluid interface should cancel each other. Additionally, the size of the local slip length is unknown for specific surfaces. To tailor specific surface characteristics and to predict the EOF on classic superhydrophobic surfaces as well as on surfaces with arbitrary liquids filling the indentations [10], these points are essential.

In this work, a scenario that should allow for a giant amplification of electro-osmotic flow along superhydrophobic surfaces is analyzed. Based on a specific principle for charge generation at the fluid-fluid interfaces, analytical expressions for the EOF velocity over a structured surface are derived that take into account the actual geometric structure of the surface.

II. EFFECTIVE BOUNDARY CONDITIONS FOR TWO-DIMENSIONAL PERIODIC SURFACES

In the following, expressions for the net electro-osmotic flow along two-dimensional (2D) periodic surfaces are derived. It is assumed that an electrolyte wets the surface in the Cassie state. The fluid filling the grooves is assumed to be nonconductive. The calculations are performed for a surface with a striped surface pattern, such as the grooves of width b and periodicity L depicted in Fig. 1. However, the resulting equations are not limited to rectangular grooves, but are correspondingly valid for all 2D periodic surfaces, where the fluid-fluid interface can be modeled by a constant-shear condition.

To eliminate the shortcoming of a vanishing net charge density at the fluidic interface, electrodes are assumed to be embedded within the surface. Upon application of a potential difference between the electrodes and the electrolyte, charges will be drawn to the fluid-fluid interfaces to shield the electric field [11], resulting in a net charge of the interface of [12,13]

$$\sigma = -\epsilon_2 E_{y,2}|_{y=0}. \tag{1}$$

Here, ϵ_2 is the permittivity of fluid 2, which fills the indentations, and $E_{y,2}$ is the y component of the electric field in fluid 2. It is furthermore assumed that the Debye length of the shielding layer developing at the interfaces is much smaller than the groove width, so that the equilibrium charge distribution can be employed within the charge layer. At small Péclet numbers and in the thin Debye layer limit, solely the classic electro-osmotic flow determines the velocity, whereas contributions due to ion concentration gradients along the surface are negligible [14,15]. Such surface conduction effects may occur in principle in the case of transverse flow, since the surface charge varies in the flow direction. They are absent in the longitudinal case. The capillary number is supposed to be small enough for the fluid-fluid interfaces to be flat.

To compute the net EOF velocity, the Lorentz reciprocity theorem [16] is employed. It reads

$$\int_S (p\hat{\mathbf{u}} - \hat{p}\mathbf{u}) \cdot \mathbf{n}\, dS = \eta \int_S (\hat{\mathbf{u}} \times \nabla \times \mathbf{u} - \mathbf{u} \times \nabla \times \hat{\mathbf{u}}) \cdot \mathbf{n}\, dS, \tag{2}$$

where S is the surface of an integration volume V (cf. Fig. 1) and $\mathbf{n}$ is the respective normal vector. p is the pressure and

*schoenecker@mpip-mainz.mpg.de

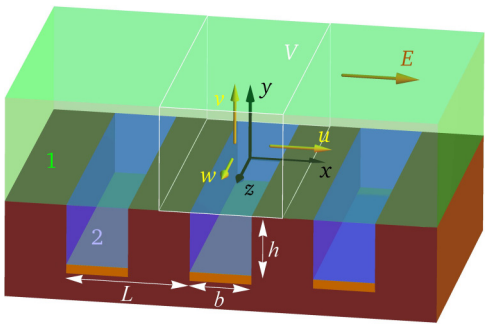

FIG. 1. (Color online) Schematic of the structured surface with embedded electrodes at the bottom of the grooves.

η is the viscosity. $\mathbf{u} = (u,v,w)$ refers to the EOF of fluid 1 and $\hat{\mathbf{u}} = (\hat{u},\hat{v},\hat{w})$ refers to a shear-driven flow along the same surface. Both flow fields fulfill the Stokes equations. The shear flow shall be driven by a shear stress τ_∞ at $y \to \infty$. If not stated otherwise, variables without a subscript refer to fluid 1.

The fluid volume V to be integrated over is chosen to extend over a spatial period in the x direction, and in the y direction from the interface at $y = 0$ to $y \to \infty$, or at least far enough away from the surface for the flow to be considered uniform. In the z direction, translational invariance is assumed, so the z extension of V is of no relevance. We consider flow in the longitudinal and transverse directions relative to the grooves. In the following, the derivation is presented for transverse flow, however all arguments apply to longitudinal flow as well.

At the wall, the velocity is given by the no-slip condition $\hat{u} = 0$ for the shear flow and by the Helmholtz-Smoluchowski equation for the EOF. In the framework of the Debye-Hückel approximation, the ζ potential at the surface can be related to the charge in the diffusive part of the double layer σ_w by $\epsilon_1\zeta = -\sigma_w\lambda_D$ [17,18], so that the Helmholtz-Smoluchowski equation reads $u = \sigma_w\lambda_D E_x/\eta_1$, with the Debye length λ_D, the electric field driving the electro-osmotic flow E_x, and the viscosity of fluid 1 η_1. The subscript w refers to the wall sections.

At the fluid-fluid interface, without loss of generality, a Navier slip condition for fluid 2 is introduced via

$$u_2(x,0) = \gamma_t(x)\left.\frac{\partial u_2}{\partial y}\right|_{y=0} \tag{3}$$

with the local slip length distribution $\gamma_t(x)$. In the case of longitudinal flow, a corresponding distribution $\gamma_l(x)$ applies. For the shear-driven flow, continuity of velocity and shear stress at the interface lead to

$$\hat{u}(x,0) = N\gamma_t(x)\left.\frac{\partial \hat{u}}{\partial y}\right|_{y=0}, \tag{4}$$

where $N = \eta_1/\eta_2$ is the viscosity ratio of the two fluids. Regarding the EOF, in the thin Debye layer limit the charge layer can be represented by a jump condition for the velocity $u_1 - u_2 = \sigma_f\lambda_D E_x/\eta_1$, resembling the Helmholtz-Smoluchowski equation at the wall (cf. [12,13]). Correspondingly, σ_f denotes the area charge density representing the Debye layer at the fluid-fluid interface, that is, the net charge of the interface. It could be induced via embedded electrodes as discussed in the context of Eq. (1). The corresponding jump condition for the shear stress at the interface is $\eta_1\,\partial u_1/\partial y - \eta_2\,\partial u_2/\partial y = -\sigma_f E_x$, so that the condition for the electro-osmotic velocity at the interface reads

$$u(x,0) = \frac{\sigma_f\lambda_D E_x}{\eta_1}\left(1 + N\frac{\gamma_t(x)}{\lambda_D}\right) + N\gamma_t(x)\left.\frac{\partial u}{\partial y}\right|_{y=0}. \tag{5}$$

Taking into account the symmetries of the problem, integration of the Lorentz reciprocity theorem (2) analogously to [7,19] yields a relation between the electro-osmotic velocity far from the surface and the flow field at the surface in the shear-driven case.

Here, we model the velocity $\hat{u}$ as a superposition of a Couette flow and flow over patches with infinite local slip length within a no-slip wall:

$$\hat{u} = (1-s)\,u_C + s u_P. \tag{6}$$

Both u_C and u_P shall be driven by the same shear stress τ_∞ at $y \to \infty$. In this case, the parameter s can be interpreted as an imperfection factor characterizing the difference between a real surface and an idealized one with an inviscid fluid enclosed in the indentations. Accordingly, the effective slip length is given by the respective fraction of effective slip length in the perfectly slipping case: $\beta_{eff} = s\beta_P$. In [20] it was shown that an ansatz of Eq. (6) is able to represent the flow field over a surface with rectangular grooves very well. The ansatz may also be suited for other types of surfaces geometries. Unlike typical assumptions of a piecewise constant local slip length, this ansatz ensures a continuous local slip length distribution $\gamma(x)$ along the surface. For rectangular grooves, the imperfection factor is given by

$$s = \begin{cases} s_t = \frac{C_t}{1+C_t} & \text{in the transverse case,} \\ s_l = \frac{C_l}{1+C_l} & \text{in the longitudinal case,} \end{cases} \tag{7}$$

with

$$C_t = \frac{4\pi a D_t N}{\ln\left(\frac{1+\sin(\frac{\pi}{2}a)}{1-\sin(\frac{\pi}{2}a)}\right)} \quad \text{and} \quad C_l = \frac{2\pi a D_l N}{\ln\left(\frac{1+\sin(\frac{\pi}{2}a)}{1-\sin(\frac{\pi}{2}a)}\right)}. \tag{8}$$

The maximum of the local slip length $\gamma(x)$ is denoted by D and can be modeled as a function of the slipping interface $a = b/L$ and the aspect ratio of the grooves, $A = h/b$ [20]. The velocity in the perfectly slipping scenario u_P is that of Philip [21,22].

Utilizing the ansatz (6) in the integrals of the Lorentz reciprocity theorem yields the EOF velocity far from the wall. For transverse flow,

$$u_{EOF} = \frac{\sigma_w\lambda_D E_x}{\eta_1}[1-(1-s_t)a] + \frac{\sigma_f\lambda_D E_x}{\eta_1}\left((1-s_t)a + s_t\frac{\beta_{t,P}}{\lambda_D}\right). \tag{9}$$

In a completely analogous manner, the longitudinal flow is

$$w_{EOF} = \frac{\sigma_w\lambda_D E_z}{\eta_1}[1-(1-s_l)a] + \frac{\sigma_f\lambda_D E_z}{\eta_1}\left((1-s_l)a + s_l\frac{\beta_{l,P}}{\lambda_D}\right). \tag{10}$$

These equations provide the possibility to determine the effects of the surface geometry, specifically of the fluid-fluid interface fraction and of the aspect ratio of the grooves, as well as of the viscosity of the enclosed fluid on the net EOF. The form of Eqs. (9) and (10) is not restricted to rectangular grooves, but applies to all surfaces with an arbitrary, periodic structure, for which the flow can be modeled as a superposition of a Couette flow and flow over alternating no-slip and no-shear patches. Consequently, if for a certain surface the effective slip length is known (e.g., through experiments), s can be determined though $\beta_{\text{eff}} = s\beta_{\text{P}}$, and the net EOF at this surface follows accordingly. Several results for flow over no-slip and no-shear patches are available, such as Philip's for grooves [21] or Davis' and Lauga's for posts [23].

For specific choices of the imperfection parameters s_t and s_l, Eqs. (9) and (10) reduce to known solutions [7,9] in which the boundary conditions at the fluid-fluid interface are introduced in a schematic manner. For example, in the case of perfectly slipping fluid-fluid interfaces ($s = 1$), Eq. (9) reduces to

$$u_{\text{EOF}} = \frac{\sigma_{\text{w}}\lambda_{\text{D}}E_x}{\eta_1} + \frac{\sigma_{\text{f}}\lambda_{\text{D}}E_x}{\eta_1}\frac{\beta_{\text{t,P}}}{\lambda_{\text{D}}}. \tag{11}$$

In the opposite case of a vanishing slip ($s = 0$), the effective velocity resulting from Eq. (9) is

$$u_{\text{EOF}} = -\frac{\epsilon_1\zeta_{\text{w}}E_x}{\eta_1}(1-a) - \frac{\epsilon_1\zeta_{\text{f}}E_x}{\eta_1}a. \tag{12}$$

This is the expected result for flow over a solid wall that is patterned with stripes of different ζ potential (cf. [24]). Schematic studies employing a constant local slip length [9] approach Eq. (12) only asymptotically in the limit of a small local slip length.

The schematic modeling of structured surfaces may lead to unrealistic results. In [9], the counterintuitive result is pointed out that for uncharged air-water interfaces, the attained EOF is greater for transverse than for longitudinal flow. By contrast, the equations for the effective electro-osmotic velocity equations (9) and (10) together with the expressions for s_t and s_l from (7) and (8) provide the possibility to investigate specific surfaces. Real grooved surfaces exhibit an anisotropic local slip [20], which is due to the flow of the secondary fluid in the cavity, while the usual schematic assumption is an isotropic local slip length as in [9]. Upon considering this anisotropy, the behavior reported in [9] can no longer be observed.

III. ESTIMATION OF THE STABILITY OF THE CASSIE STATE

Electro-osmotic flow enhancement on superhydrophobic surfaces relies on the fact that the liquid is in the Cassie state. In the common case of a purely hydrodynamic flow without electrical forces, the Cassie-to-Wenzel transition is induced if the pressure difference across the fluid-fluid interface becomes too high. Here, we focus on the general properties of the Cassie-to-Wenzel transition under the influence of electric fields. In this case, it is the electric field normal to the interface that leads to a deformation of the same.

Let us estimate the stability limits for a grooved surface. A corresponding unit cell is depicted in Fig. 2. The deflection of

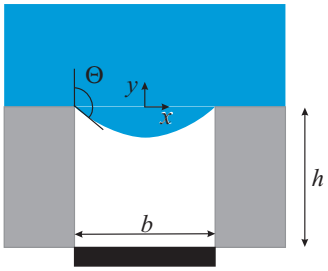

FIG. 2. (Color online) Schematic of a deflected fluid-fluid interface.

the interface shall be described by $g(x)$. Then, $g(x)$ is related to the contact angle (Fig. 2) via

$$\Theta = 90^\circ - \frac{360^\circ}{2\pi}\arctan\left(\frac{dg}{dx}\right)\bigg|_{x=-b/2}. \tag{13}$$

For simplicity, we assume the interface has a trigonometric shape of

$$g(x) = \alpha\cos\left(\frac{\pi}{b}x\right). \tag{14}$$

During the deflection process, the shape of the interface may change. More accurate results should be obtained when extending $g(x)$ to a Fourier series. Here, mainly the basic principle of the instability is of interest, therefore only the first element of the series is considered.

A. Electrical breakdown

If the electric field within the groove exceeds the breakdown electric field of the respective medium filling the groove, the originally insulating fluid starts to become conducting. Plasma discharges may occur, for example in the form of sparks. The breakdown limit is usually given in terms of the breakdown voltage U_{b}. For gases, it is given by the Paschen law [25] (see also [26,27]):

$$U_{\text{b}} = \frac{Bpd}{\log(Apd) - \log\left[\log\left(1+\frac{1}{\gamma}\right)\right]}, \tag{15}$$

illustrating the dependence of the breakdown voltage on the product of the pressure and the gap size pd. The coefficients A, B, and γ are material parameters originating from the description of different ionization processes. For air at atmospheric pressure and within the considered range of the electric field, we may set $A = 645\ \text{mm}^{-1}\,\text{bar}^{-1}$, $B = 19\ \text{kV}\,\text{mm}^{-1}\,\text{bar}^{-1}$, and $\gamma = 0.02$ [27]. Additionally, the breakdown voltage depends on effects such as the humidity of the air and the shape of the electrodes. For the present estimation, the gap size is taken as $d = h + \alpha$, i.e., the closest distance between the interface and the bottom of the groove.

The breakdown electric field strength is not the same for micrometer-sized grooves as for large gaps. At macroscopic gap sizes, the breakdown electric field strength of air at atmospheric pressure is about 2.5–3 kV/mm. For gap sizes in the micrometer range, which is the case for a microstructured surface, the breakdown electric field strength increases to about twice this value at a gap size of 100 μm and to about

five times the value at a size of 20 μm. This behavior is of course beneficial, as an increased electric field invokes a greater induced surface charge and ultimately a greater electro-osmotic velocity. The Paschen law is valid up to gap sizes of about 4 μm [28,29]. For liquids, corresponding theories for the breakdown voltage exist [30].

B. Depinning

Without the application of an electric field, the fluid-fluid interface is ideally flat. The contact line is pinned at the edges of the cavity. If the electric field is increased, the interface deforms, so that the forces due to Maxwell stresses and to the surface curvature balance. Upon the contact angle of the fluid-fluid interface exceeding the advancing contact angle of the specific wall material, the contact line starts to move down into the groove.

C. Interface instability

Before the interface deforms to an extent that the advancing contact angle is reached, it might become unstable if the capillary pressure is no longer able to balance the Maxwell stress. Then the system may undergo a transition to a configuration of lower free energy, similar to processes occurring in electrospraying. A relation for the maximum deflection α as a function of the potential between the bottom of the groove and the electrolyte U as well as a stability criterion for the interface can be obtained by considering the energy balance of the system.

Upon deflection, the surface energy varies with the arc length B of the fluid-fluid interface as

$$W_s \sim \sigma B = \sigma \int_{-b/2}^{b/2} \sqrt{1+\left(\frac{dg}{dx}\right)^2}\, dx = \frac{2b\sigma}{\pi} E\left(-\frac{\pi^2\alpha^2}{b^2}\right). \tag{16}$$

In this equation, the function $E(m)$ is the complete elliptic integral of the second kind and should not be confused with the electric field. At small deflections, the electric field is approximately

$$E_y(x) = \frac{U}{-h-g(x)}, \tag{17}$$

with the highest electric field occurring at the point of greatest deflection, $x = 0$.

The electrostatic energy can be estimated by

$$W_{el} \sim \frac{1}{2}\epsilon_2 \int_{-b/2}^{b/2}\int_{-h}^{g(x)} E_y^2\, dx\, dy \sim -\frac{2b\epsilon_2 U^2}{\pi\sqrt{h^2-\alpha^2}} \arctan\left(\sqrt{\frac{2h}{h+\alpha}-1}\right). \tag{18}$$

Upon application of a potential U, the system reacts with a deflection α that corresponds to the minimum free energy, hence to $\partial(W_s + W_{el})/\partial\alpha = 0$. This equation yields an implicit expression for the deflection,

$$U = \frac{i\sqrt{2}(\alpha^2-h^2)\sqrt{\sigma\left[E\left(-\frac{\pi^2\alpha^2}{b^2}\right)-K\left(-\frac{\pi^2\alpha^2}{b^2}\right)\right]}}{\sqrt{\alpha\epsilon_2\left[-\alpha^2-2\alpha\sqrt{h^2-\alpha^2}\arctan\left(\sqrt{\frac{2h}{\alpha+h}-1}\right)+h^2\right]}}, \tag{19}$$

with the complete elliptic integral of the first kind $K(m)$. Equation (19) exhibits a stable branch, corresponding to the energy minima, and an unstable branch, corresponding to the maxima. The system follows the stable branch until, at the point of instability, it meets the unstable branch. The overall energy is then monotonically decreasing with increasing deflection.

The present estimation of the free energy follows principles similar to those employed by Oh et al. [31] for circular cavities. They assumed a parabolic shape of the interface and restricted their analysis to the depinning and interface instability mechanisms. Here, the electrical breakdown limit has also been taken into account. Equation (19) is an estimation and demonstrates the principle of the stability limits.

Examples of the stability limits for two superhydrophobic surfaces with rectangular grooves are shown in Fig. 3. The wall material is taken to be polytetrafluoroethylene (PTFE) with an advancing contact angle of 118°. Generally, the specific groove geometry determines which limiting curve or point the deflection curve crosses first. The estimation rather overestimates the actual deflection. Varying the geometry shows that electrical breakdown is a major limit. The comparatively large contact angle of PTFE avoids depinning, a threshold that would vary correspondingly with the substrate material. In practice, further effects such as impurities or rounded corners would of course additionally influence the wetting behavior, at least locally.

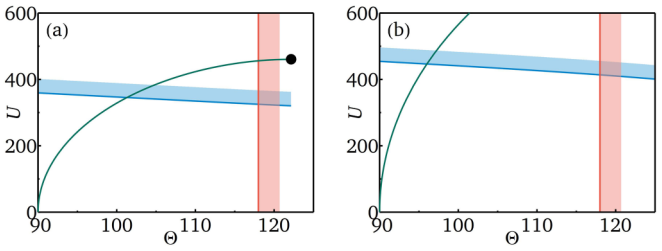

FIG. 3. (Color online) Stability of the Cassie state under the influence of an electric field normal to the fluid-fluid interface. Example of a PTFE surface with air filling the grooves of width × depth: (a) 50 × 30 μm; (b) 50 × 50 μm. Green: deflection with applied voltage; blue: electrical breakdown limit; red: depinning limit; black point: surface instability limit.

IV. EOF ENHANCEMENT FOR RECTANGULAR GROOVES

Overall, Eqs. (9) and (10) allow a rather universal investigation of EOF on different types of structured surfaces with a fluid in the Cassie state. We will now specifically examine rectangular grooves. The EOF enhancement factor is defined

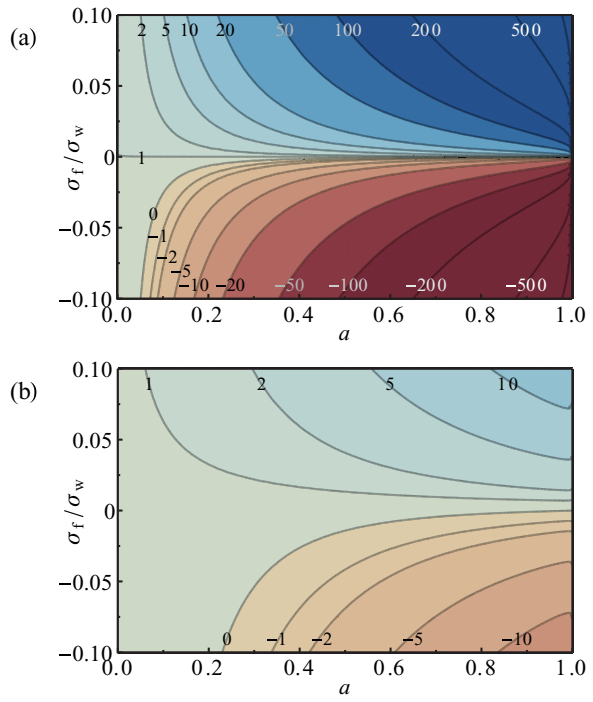

FIG. 4. (Color online) Enhancement factor for the longitudinal electro-osmotic velocity over a grooved surface relative to that over a plain wall for $A = 1$, $L/\lambda_D = 10^4$: (a) water flowing over air ($N \approx 55.56$); (b) water flowing over a viscous liquid ($N \approx 0.056$).

as

$$\frac{u_{EOF}}{u_{ref}} = 1 + (1 - s_t)\, a \left(\frac{\sigma_f}{\sigma_w} - 1 \right) + \frac{\sigma_f}{\sigma_w} \frac{L}{\lambda_d} s_t \beta^*_{t,P}, \qquad (20)$$

where u_{ref} is the EOF velocity along an unstructured, planar wall of the same material as the structured surface. Here, $\beta^*_{t,P} = \beta_{t,P}/L$ is the normalized effective slip length of Philip [22]. The enhancement factor in the longitudinal case w_{EOF}/w_{ref} follows analogously.

Figure 4 illustrates the effect of a net charge at the fluid-fluid interface and the area fraction of this interface on the flow enhancement factor in the longitudinal case, exemplarily for the cases of air ($\eta_2 = 1.8 \times 10^{-5}$ Pa s) and a viscous liquid ($\eta_2 = 1.8 \times 10^{-2}$ Pa s) filling the grooves. The aspect ratio of the grooves was set to $A = 1$, where the slip length has generally reached its maximum value for the respective a, and the ratio of period and Debye length was $L/\lambda_D = 100\ \mu m/10\ nm = 10^4$.

For a standard superhydrophobic surface [Fig. 4(a)], quite high enhancement factors are predicted already for very low net charge densities at the fluid-fluid interface. It is obvious that a high fluid-fluid interface fraction is essential for a large amplification of the velocity. At high a, the velocity strongly increases with the magnitude of σ_f/σ_w, whereas at low a, the charge density can virtually be arbitrarily increased without a significant effect. At vanishing interface charge, the relative velocity is closely below 1, as the viscosity ratio is high. If σ_f takes the opposite sign of σ_w, the flow may be reversed. With increasing fluid-fluid interface fraction, the flow in the opposite direction over the wall is negligible. In this regime, the diagrams are nearly symmetric with respect to the line $\sigma_f/\sigma_w = 0$. Transverse flow behaves fully analogously. The amplification factors are close to twice as large in the longitudinal case compared to the transverse case. This corresponds to the relation between the effective slip lengths for shear-driven flow in these two cases.

A typical scenario considered with the schematic models is the case in which the fluidic interface has the same ζ potential as the wall. Within the Debye-Hückel approximation (i.e., $\epsilon_1 \zeta = -\sigma \lambda_D$), this corresponds to $\sigma_f/\sigma_w = 1$. Figure 4 shows that large EOF enhancement factors are already achieved for much smaller interface charge densities. Besides that, real interfaces will usually not support charge densities as high as $\sigma_f/\sigma_w = 1$. Referring to the scheme for charge generation depicted in Fig. 1, Maxwell stresses may deform the fluidic interface and eventually destroy the Cassie state as described in the previous section.

The maximum achievable net surface charge density σ_f depends on the maximum electric field in the groove. If we assume this to be given by the breakdown electric field strength, typical values for the maximum charge density ratio at a classic superhydrophobic surface with wall potential $\zeta_w = -50$ mV are about $\sigma_f/\sigma_w \approx 0.1$ for 10 μm deep grooves and $\sigma_f/\sigma_w \approx 0.015$ for 100 μm deep grooves. At such a surface, grooves of $b = 50\ \mu m$, $h = 20\ \mu m$, and $a = 0.9$ would lead to a maximum enhancement factor of about 250. With lower values of ζ_w, the enhancement factor increases further. At greater a, which in particular might be achieved with alternative surfaces geometries (see, e.g., [32]), even greater enhancements are expected.

Another influencing factor is that a curved interface may also reduce the slip length. Since the parameter s characterizes the effective slip length of a real surface relative to that of the ideal surface, it can be estimated from the reduction in effective slip length obtained in previous work on flow over surfaces with curved interfaces. For a surface with an advancing contact angle of 118°, Ref. [33] suggests a value of s_t of the order of 0.8. However, in most of the cases the electrical breakdown limit will not allow for such a large deformation. Correspondingly, $s_t \approx 0.95$ for the geometry of Fig. 3(b), where the deflection is probably still overestimated. From Eq. (20), a reduction of the EOF of the same order of magnitude results. For longitudinal flow over the same surface, the losses due to interface deformation are expected to be even smaller.

At a less favorable viscosity ratio than that of a classic superhydrophobic surface, the achievable EOF enhancement factor is much lower [Fig. 4(b)]. At zero fluid-fluid interface potential, the velocity is strongly reduced for real fluids compared to an EOF along a planar wall. The higher the viscosity of the medium filling the grooves, the greater σ_f/σ_w must be to achieve considerable velocity amplifications. This agrees with experiments on influencing electro-osmotic flow by embedded electrodes underneath a solid wall [34–37], i.e., the limiting case of very high viscosity, where very high voltages are needed in order to have any impact on the flow. Although the maximum charge density at the fluid-fluid interface may be higher for liquid-filled than for gas-filled grooves by the ratio of the permittivities of the groove-filling media, fluid permittivities are usually not large enough to compensate for the effect of viscosity.

V. CONCLUSIONS

In summary, Eqs. (9) and (10) provide effective boundary conditions for the transverse and longitudinal electro-osmotic flow along periodically structured surfaces with an arbitrary dielectric fluid filling the indentations. They are valid for flow over all periodic surface structures that can be modeled by a superposition of Couette flow and flow over no-slip and no-shear patches. Specifically, for a surface with rectangular grooves, the influence of the groove dimensions as well as the viscosity of the fluid inside the grooves is taken into account. High amplification factors for the electro-osmotic velocity are predicted already for low charge densities at the fluid-fluid interfaces. On a suitably designed superhydrophobic surface with auxiliary electrodes, an amplification of the EOF by more than two orders of magnitude can be expected. The expressions for the net electro-osmotic velocity provide a basis for the investigation and understanding of such flows as well as for the development and design of novel surfaces, e.g., with alternative fluids filling the surface indentations.

ACKNOWLEDGMENTS

We acknowledge funding by the Deutsche Forschungsgemeinschaft through the Cluster of Excellence "Center of Smart Interfaces" and the Graduate School "Computational Engineering."

[1] E. Lauga and H. A. Stone, J. Fluid Mech. **489**, 55 (2003).
[2] M. Sbragaglia and A. Prosperetti, J. Fluid Mech. **578**, 435 (2007).
[3] J. Eijkel, Lab Chip **7**, 299 (2007).
[4] D. M. Huang, C. Cottin-Bizonne, C. Ybert, and L. Bocquet, Phys. Rev. Lett. **101**, 064503 (2008).
[5] P. Tsai, A. M. Peters, C. Pirat, M. Wessling, R. G. H. Lammertink, and D. Lohse, Phys. Fluids **21**, 112002 (2009).
[6] C.-O. Ng and C. Y. Wang, Fluid Dyn. Res. **43**, 065504 (2011).
[7] T. M. Squires, Phys. Fluids **20**, 092105 (2008).
[8] H. Zhao, Phys. Rev. E **81**, 066314 (2010).
[9] A. V. Belyaev and O. I. Vinogradova, Phys. Rev. Lett. **107**, 098301 (2011).
[10] T.-S. Wong, S. H. Kang, S. K. Y. Tang, E. J. Smythe, B. D. Hatton, A. Grinthal, and J. Aizenberg, Nature (London) **477**, 443 (2011).
[11] C. Steffes, T. Baier, and S. Hardt, Colloids Surf. A **376**, 85 (2011).
[12] L. D. Landau and E. M. Lifshitz, *Course of Theoretical Physics, Electrodynamics of Continuous Media* (Pergamon, Oxford, 1960).
[13] J. R. Melcher and G. I. Taylor, Annu. Rev. Fluid Mech. **1**, 111 (1969).
[14] A. S. Khair and T. M. Squires, Phys. Fluids **20**, 087102 (2008).
[15] Briefly, referring to the analysis given in [14], the flow velocity given in Eq. (37) of this reference has two components, the usual EOF velocity and a second "chemiosmotic" term that is due to gradients in the osmotic pressure. In the following, this term will be denoted by u_{osm}. The wall geometry we consider is not only periodic with period L, it is also symmetric under $x \to -x$. If the Péclet number is small enough, the salt concentration in the bulk (i.e., outside of the Debye layer) will not be perturbed by the flow, i.e., it will also be symmetric under $x \to -x$. Then, due to the derivative with respect to x [14], u_{osm} will be antisymmetric under $x \to -x$. Specifically, $u_{\mathrm{osm}}(-x) = -u_{\mathrm{osm}}(x)$. This means that the integral of u_{osm} over one period L vanishes. Therefore, this term does not give any contribution to the net EOF velocity observed far away from the structured surface.
[16] H. A. Lorentz, *Abhandlungen über Theoretische Physik* (Teubner, 1907), pp. 23–42, revised version of Eene Algemeene Stelling Omtrent de Beweging Eerier Vloeistof met Wrijving en Eenige Daamit Afgeleide Gevolgen (Zittingsverslag van de Koninklijke Akademie van Wetenschappen te Amsterdam, 1896), Vol. 5, pp. 168–175. A translation of the original version in English appeared in J. Eng. Math. **30**, 19 (1996).
[17] V. G. Levich, *Physicochemical Hydrodynamics* (Prentice-Hall, Englewood Cliffs, NJ, 1962).
[18] D. J. Shaw, *Introduction to Colloid and Surface Chemistry* (Butterworths, Oxford, 1980).
[19] T. Baier, C. Steffes, and S. Hardt, Phys. Rev. E **82**, 037301 (2010).
[20] C. Schönecker, T. Baier, and S. Hardt, J. Fluid Mech. **740**, 168 (2014).
[21] J. R. Philip, Z. Ang. Math. Phys. (ZAMP) **23**, 353 (1972).
[22] J. R. Philip, Z. Ang. Math. Phys. (ZAMP) **23**, 960 (1972).
[23] A. M. J. Davis and E. Lauga, J. Fluid Mech. **661**, 402 (2010).
[24] A. Ajdari, Phys. Rev. E **53**, 4996 (1996).
[25] F. Paschen, Ann. Phys. **273**, 69 (1889).
[26] J. Meek and J. Craggs, *Electrical Breakdown of Gases* (Oxford University Press, Oxford, 1953).
[27] Y. P. Raizer, *Gas Discharge Dynamics* (Springer, Berlin, 1991).
[28] L. H. Germer, J. Appl. Phys. **30**, 46 (1959).
[29] R. S. Dhariwal, J.-M. Torres, and M. P. Y. Desmulliez, Sci. Meas. Technol. IEE Proc. **147**, 261 (2000).
[30] D. W. Swan, Proc. Phys. Soc. **78**, 423 (1961).
[31] J. M. Oh, G. Manukyan, D. van den Ende, and F. Mugele, Europhys. Lett. **93**, 56001 (2011).
[32] C. Lee, C.-H. Choi, and C.-J. "CJ" Kim, Phys. Rev. Lett. **101**, 064501 (2008).
[33] A. M. J. Davis and E. Lauga, Phys. Fluids **21**, 011701 (2009).
[34] M. A. Hayes and A. G. Ewing, Anal. Chem. **64**, 512 (1992).
[35] C. T. Wu, C. S. Lee, and C. J. Miller, Anal. Chem. **64**, 2310 (1992).
[36] E. J. van der Wouden, T. Heuser, D. C. Hermes, R. E. Oosterbroek, J. G. E. Gardeniers, and A. van den Berg, Coll. Surf. A **267**, 110 (2005).
[37] C. Pirat, A. Naso, E. J. van der Wouden, J. G. E. Gardeniers, D. Lohse, and A. van den Berg, Lab Chip **8**, 945 (2008).